Desalination and Water Treatment
www.deswater.com

doi:10.5004/dwt.2017.21396

88 (2017) 93–105
September

Studies on the removal of manganese from synthetic wastewaters by nanofiltration– a parametric and modeling study

Deepti S. Patil[a], John U. Kennedy Oubagaranadin[b], Sanjay M. Chavan[c,*]

[a]*Faculty of Chemical Engineering, Visvesvaraya Technological University, Belagavi - 590018, Karnataka, India, Tel.+919822635605, email: deepti_pat@rediffmail.com*
[b]*Department of Ceramic and Cement Technology, PDA College of Engineering, Gulbarga – 585102, Karnataka, India, Tel. +919449638617, email: jukennedy@gmail.com*
[c]*Department of Chemical Engineering, Sinhgad College of Engineering, Pune – 411041, Maharashtra, India, Tel.+ 917875577039, Fax +91 020 24357243, email: drsmchavan22@gmail.com*

Received 22 April 2017; Accepted 28 August 2017

ABSTRACT

Due to the current environmental legislations, treatment of the industrial wastewater containing heavy metals is a problem of critical significance. Among the heavy metals, manganese is a very common contaminant of the industrial wastewater. In the present work, removal of manganese from the synthetic industrial wastewater was studied using the commercially available hydrophilized polyamide (HPA-400) nanofiltration membrane in the spiral wound module. The feed concentration (20–100 mg/L), the transmembrane pressure (TMP) (5–9 bar), and the feed flow rate (0.713–1.050 L/min) were used as the operating parameters to explore the influence on the membrane performance. It was found that the observed rejection of manganese increased with the increase in the initial feed concentration, the transmembrane pressure, and the feed flow rate. Experiments were carried out using Taguchi design of experiments(DOEs) method. The statistical analyses of the experimental results in terms of the signal-to-noise ratio (S/N ratio) and the analysis of variance (ANOVA) showed that the feed concentration was the most significant factor affecting the rejection of metal, followed by the transmembrane pressure and then the feed flow rate. The highest observed rejection of manganese was found to be 92.58% for the initial feed concentration of 100 mg/L, the transmembrane pressure of 9 bar and the feed flow rate of 1.050 LPM. The statistical model was developed and validated using the experimental data. For theoretical modeling study, the well-known combined-film-theory-Spiegler-Kedem model (CFSK) was used to estimate the membrane transport parameters. The Sherwood correlation was also developed for the spiral wound membrane module under the studies. Furthermore, the enrichment factors, concentration polarization modulus, as well as Peclet numbers were computed.

Keywords: Manganese; Rejection; Nanofiltration; Membrane; Taguchi technique

1. Introduction

With the rapid development of industries and present environmental related legislations, a number of environmental problems need to be solved. As the present operating techniques cannot be changed completely, the protective environmental strategy cannot be enforced. Many industries like metal finishing, electroplating, and electrochemical processes discharge liquid waste with high concentrations of metals. Thus, it is essential to get rid of them before releasing it into natural bodies of water. It is a known fact that heavy metals do not decompose easily and completely. Their traces are carried through various life cycles. So, they are considered extremely toxic and carcinogenic [1].

Among the heavy metals, manganese is of great importance. It is generally used in ferrous metallurgy apart from chemical, electrochemical, food, and pharmaceutical appli-

*Corresponding author.

cations [2]. The extravagant use of manganese containing products, the industries with a high concentration of manganese in the effluents like mining [3], and steel manufacturing industries [4] lead to environmental pollution at dangerous levels. In natural resources also, manganese is available. Specifically, by the weathering of manganese-rich rocks and sediments, manganese occurs universally in low levels in soil, water, air, and nutrient. Lack of manganese in human beings seems to be exceptional since it exists in a variety of nutrients. It is of the essence for the normal bone structure, and good brain function. It is indispensable for the proper functioning of some enzymes (manganese superoxide dismutase, pyruvate carboxylase) and for the stimulation of others (kinases, decarboxylases, transferases, hydrolases, etc.).For the adults, WHO (1973) decided that the manganese intake of 2–3 mg/d is sufficient and 8–9 mg/d is "perfectly safe".The manganese intake from the drinking-water is generally lower than the intake from the food. The intake of manganese through the water would be 20 μg/d for an adult, considering a daily water intake of 2 L [5].

Although manganese is a significant nutrient at low doses, prolonged exposure to higher doses may be harmful. The concentration of manganese over 0.1 mg/L in the water supplies, creates an unwanted taste in the beverages and blemishes the sanitary ware and laundry. The occurrence of manganese (II) in the drinking water may build up its concentration biologically [6]. Manganese accumulates in the tissues where mitochondria and endoplasmic reticulum are present abundantly. The main sites of accumulation after the skeleton are the liver, pancreas, kidneys, skeletal muscle, connective tissue, and intestine [7]. It occurs when insufficient disinfectant residual is present in the distribution system to control the growth of manganese depositing biofilm [8].

The water quality standards and the various techniques used over the period for the removal of Mn ions from wastewaters have been discussed in our review paper [9]. These techniques are precipitation, ion exchange, coagulation/flocculation, oxidation-filtration, electrochemical and biological processes, adsorption and membrane techniques.

The presence of manganese in the industrial effluents has been increased considerably. Specifically, in the acid mine drainage, manganese occurs at much higher concentrations than the recommended discharge values. Usually, the divalent form, Mn(II) is soluble in water. In the acid mine drainage, the divalent species are predominant up to pH 10. The need of increasing the pH above 10, in order to meet the standard limits, usually < 1 mg/L, is a problem for discharging [10]. Another problem associated with this increase in pH along with the oxygenation of the system is it produces different forms of the solid manganese [11]. In addition, it involves a high consumption of reagents. For the effective precipitation also, a pH higher than 10 is required due to the high solubility of Mn(II) in a wide pH range [12]. Thus, the removal of manganese from the mining industry effluent is a major challenge for the water management, as manganese is not removed by pH control alone [13].

Manganese generally coexists with iron in the groundwater. For the treatment of the groundwater containing manganese and iron, oxidation can be used because, after oxidation of Mn(II) compounds, Mn(IV) compounds are formed. These Mn (IV) compounds are insoluble. Conventional treatment for the removal of iron and manganese from the groundwater is oxidation followed by depth filtration. But, this process works efficiently when there is no dissolved organic matter and the total concentration of Fe(III) and Mn(II)is less than 5 mg/L. For the higher concentrations, excessive amounts of the solids tend to shorten filtration cycles and make the whole process ineffective. Additionally, the ability of filtration of the manganese oxides is very low and control over the process may be challenging with variations in the raw water quality. The alternative process recommended is the membrane filtration in which two options are the direct membrane treatment and the combination of oxidation with the membrane separation [14]. Many investigators used the combination of oxidation and microfiltration for the removal of iron and manganese from the groundwater [14–17]. However, the kinetics of Mn (II) oxidation are very slow [18]. Additionally, due to the high redox potential of Mn(IV), the parallel reactions such as organic matter and Fe(II) oxidation, result in excessive oxidant consumption. Therefore, removal of iron is necessary before the manganese oxidation [19].

Among these technologies, the membrane technology is widely accepted for treating the surface water, brackish water, well water, brine and the industrial wastewater [20–22]. Microfiltration, ultrafiltration, nanofiltration and reverse osmosis are the "pressure driven membrane processes" [23]. The choice of the correct membrane method rests on the molecular size of the pollutants contained in the water [20]. Among these membrane technologies, nanofiltration (NF) can be placed between reverse osmosis and ultrafiltration. It is effective in removing the elements causing hardness of the water, such as calcium and magnesium along with the bacteria, viruses, and color [23].

The advantages of NF are good quality of the treated water, process and plant compactness and simple automation. In addition to this, NF requires only cleaning agent chemicals as compared to the other technologies in which chemical consumption (coagulants, flocculants, disinfectants, pH adjustment chemicals) is high [24]. Also, it can remove the heavy metal ions with high efficiency [1]. Many researchers have used NF for removing the heavy metals like arsenic [25], copper [26], cadmium [27], chromium [28], zinc [29], and lead [30] from the wastewater.

The key objective of the present work was to explore the removal of manganese ions from the synthetic industrial wastewater using the HPA-400 membrane. The operating parameters were the feed concentration, the transmembrane pressure, and the feed flow rate. Taguchi method was employed for the design of experiments and subsequent statistical analyses were performed by evaluating the signal-to-noise (S/N) ratio and the analysis of variance (ANOVA). The statistical model was developed using the software MINITAB® 18 version 18.1(Minitab Inc., USA). Also, the membrane transport parameters were estimated using the combined-film theory- Spiegler–Kedem model. The new Sherwood number equation was established for the spiral wound membrane module. The mass transfer coefficients obtained from the model and from the established Sherwood number correlation were compared. Similarly, the enrichment factors, concentration polarization modulus, and Peclet number were calculated for the HPA-

400 NF membrane. All the experimental data were collected at ambient (25°C) temperature.

2. Theoretical background

2.1. Film theory model

The objective for the development of the membrane mass transfer model is to relate the performance to the operating conditions. With the high flux rate, a solute which does not transfer through the membrane may accumulate at the membrane surface. This is called the concentration polarization (Fig. 1). The solute flux passing through the membrane is balanced by the forward convective transport of solute, $J_v \cdot C_A$ and the back diffusive mass transport from the membrane surface to the bulk solution, $D_{AB} \cdot (dC_A/dx)$. So, at steady state, using the film theory, a mass balance of the solute in differential form is given as:

$$N_A = C_A J_v - D_{AB}\left(\frac{dC_A}{dx}\right) \tag{1}$$

where D_{AB} is the diffusivity of the solute in the solvent (m^2/s), N_A is the solute flux ($kg/(m^2 \cdot s)$), C_A is the concentration of the solute at any location (mg/L). The boundary conditions are

(i) $C_A = C_{A1}$, at $x = 0$;
(ii) $C_A = C_{A2}$, at $x = l$;

where l is the thickness of the boundary layer (m). With the above boundary conditions, integration of Eq. (1) produces [31].

$$\left(\frac{C_{A2} - C_{A3}}{C_{A1} - C_{A3}}\right) = \exp\left(\frac{J_v}{k}\right) \tag{2}$$

where k is the mass transfer coefficient defined as (D_{AB}/l).

The observed rejection is given by

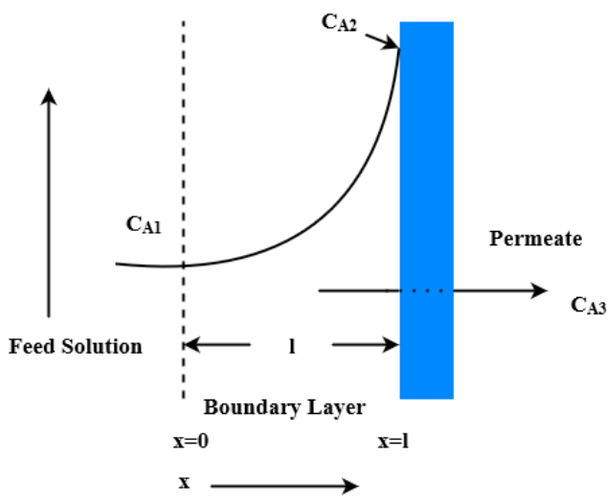

Fig. 1. Schematic of concentration gradients of the solute adjacent to the membrane surface.

$$R_o = \left[1 - \frac{C_{A3}}{C_{A1}}\right] \tag{3}$$

and the true rejection is given as:

$$R = \left[1 - \frac{C_{A3}}{C_{A2}}\right] \tag{4}$$

The concentration polarization expression [Eq. (2)] can be written in terms of the rejection coefficients by substituting these rejection coefficients at the place of concentrations to give:

$$\frac{Ro}{1 - Ro} = \left[\frac{R}{1 - R}\right]\left[\exp\left(\frac{-J_v}{k}\right)\right] \tag{5}$$

2.2. Solution-diffusion model

The solution-diffusion (SD) model was originally applied to reverse osmosis by Merten and coworkers [32]. In this model, the solute flux and the solvent flux are proportional to their chemical potential difference. The solvent and the solute fluxes, respectively are

$$J_V = A(\Delta P - \Delta\pi) \tag{6}$$

$$N_A = \left(\frac{D_{AM}K}{\delta}\right)(C_{A2} - C_{A3}) \tag{7}$$

where A is the solvent permeability parameter. It can be estimated from the pure water permeability calculation. D_{AM} is the solute diffusion coefficient in the membrane (m^2/s), K is the solute distribution coefficient in the membrane and solution, δ is the membrane thickness (m), and $(D_{AM}K/\delta)$ is the solute transport parameter.

2.3. Combined- film theory - solution-diffusion model (CFSD model)

According to the film theory model, and the solution-diffusion model, as proved by Pusch [33], Eqs. (6) and (7) may be combined with Eq. (4), to get an alternative equation of the true rejection as:

$$\frac{1}{R} = 1 + \left(\frac{D_{AM}K}{\delta}\right)\left(\frac{1}{J_v}\right) \tag{8}$$

The Eq. (8) proposes a linear relationship between $1/R$ and $1/J_v$. One restriction of the SD model is that the separation obtained at infinite flux is always equal to 1.0. However, this limit is not reached for many solutes. Thus, the SD model is suitable for the solute-solvent membrane systems where the separation is close to 1.0. Eq. (8) can be rearranged as:

$$\frac{R}{1 - R} = \left[\frac{J_v}{\frac{D_{AM}K}{\delta}}\right] \tag{9}$$

This Eq. (9) can be substituted into Eq. (5) to give

$$\frac{R_o}{1-R_o}=\left[\frac{J_v}{\frac{D_{AM}K}{\delta}}\right]\left[\exp\left(-\frac{J_v}{k}\right)\right] \tag{10}$$

Eq. (10) is the combined-film theory-solution-diffusion (CFSD) model and in the logarithmic format can be obtained as:

$$\ln\left[\frac{(1-R_o)J_V}{R_o}\right]=\ln\left[\frac{D_{AM}K}{\delta}\right]+\left(\frac{J_v}{k}\right) \tag{11}$$

A plot of ln $[(1–R_o)J_v/R_o]$ vs. J_v will give a linear relation with a slope equal to $1/k$ and the intercept equal to ln $(D_{AM}K/\delta)$ for the different feed concentrations. It can be done by using the R_o and the J_v data measured at the various transmembrane pressures, keeping the same feed flow rate and the feed concentration for each set.

2.4. Combined- film theory -Spiegler– Kedem model

When the information on the membrane structure and the morphology is not available, the theory of irreversible thermodynamics (IT) can be used in membrane systems. In IT, the membrane is treated as a "black box". The Spiegler–Kedem model (SK) is developed using the principles of irreversible thermodynamics. The basic equations of the Spiegler–Kedem model [34] are

$$J_V=L_P(\Delta P-\sigma\Delta\pi) \tag{12}$$

$$R=\frac{\sigma(1-F)}{1-\sigma F} \tag{13}$$

where

$$F=\exp\left(-\frac{(1-\sigma)}{P_M}J_V\right) \tag{14}$$

and σ is the reflection coefficient. It signifies the solute-water coupling as well as the solute rejection by the membrane. σ has values between 0 to 1. At σ = 1, the membrane is ideal, showing no solute-water coupling and the total solute rejection. At σ = 0, the membrane shows no semi-permeability and therefore, no solute rejection. L_p is the pure water permeability coefficient of the membrane, and P_M is the overall solute permeability coefficient. Eq. (13) can be written as:

$$\frac{R}{1-R}=\frac{\sigma}{1-\sigma}(1-F) \tag{15}$$

Then, combination of Eq. (15) with Eq. (5) gives

$$\frac{Ro}{1-Ro}=\frac{\sigma}{1-\sigma}\left\{1-\exp\left[-J_v\left(\frac{1-\sigma}{P_M}\right)\right]\right\}\left[\exp\left(\frac{-J_v}{k}\right)\right] \tag{16}$$

Eq. (16) is called the combined-film theory-Spiegler–Kedem (CFSK) model[31].

2.5. Enrichment factors and concentration polarization modulus

The boundary layer film model generalizes the fluid hydrodynamics taking place in the membrane modules. However, it has one parameter, the boundary layer thickness can be changed. After replacing the concentration terms by an enrichment factor E, defined as C_{A3}/C_{A1} and the enrichment obtained in the absence of a boundary layer E_o, defined as C_{A3}/C_{A2} in Eq. (2), it can be expressed as [35]:

$$\left(\frac{\frac{1}{E_0}-1}{\frac{1}{E}-1}\right)=\exp\left(\frac{J_v}{k}\right) \tag{17}$$

The level of concentration polarization can be indicated by the concentration of the solute accumulated on the membrane surface, compared to the bulk solution concentration. It is shown by the term, concentration polarization modulus defined as $C_{A2}/C_{A1.}$ This ratio increases with the increasing flux, with increasing the rejection and with decreasing the mass transfer coefficient [36]. It is assumed that the concentration polarization does not occur when the modulus is 1.0. However, it affects the membrane selectivity and the flux significantly when the modulus deviates farther from 1.0.According to the definitions of E and E_o, the concentration polarization modulus can also be represented as E/E_o and, from Eqs. (2) and (17), it can be expressed as [35]:

$$\frac{C_{A2}}{C_{A1}}=\frac{\exp\left(\frac{J_v}{k}\right)}{1+E_0\left[\exp\left(\frac{J_v}{k}\right)-1\right]} \tag{18}$$

3. Experimental

3.1. Materials

The hydrophilized polyamide HPA-400 membrane was purchased from Permionics, Vadodara, India. The membrane had an effective area of 0.4 m^2. The feed concentrations of 20–100 mg/L of Mn (II) were employed during the process operation. Manganese sulfate monohydrate ($MnSO_4{\cdot}H_2O$, MW = 169 g/mol), sodium meta-bisulphite ($Na_2S_2O_5$) and the standard manganese metal solution (1000 mg/L) were purchased from Merck. All the chemicals used for the preparation of the synthetic solutions were of the analytical reagent grade and were used as received. To avoid the interference of the other species, present in the tap water, deionized water was used to prepare the artificial Mn (II) solution, to clean the membrane set up and to prepare the analytical standard solutions. It was produced from Milli-Q Gradient unit (Millipore, conductivity 0.055 μS/cm).

The characteristics of the membrane module are shown in Table 1.

3.2. Plant setup and methods

The experiments were conducted on a Perma® membrane system (Permionics, Vadodara, India). The sche-

Table 1
Characteristics of HPA-400 nanofiltration membrane module

Parameters	Reference value
Configuration	Spiral wound, D = 2 inch, L = 12 inch
Number of membrane leaves	2
Maximum operating pressure, bar	13
Molecular weight cut off (MWCO), Da	400
Maximum operating temperature, °C	40
pH range	2–11
Chlorine tolerance	Nil

matic diagram of Perma® plant is shown in Fig. 2. The plant was equipped with a horizontal arrangement of the filtration modules supported on the metal skid. The module was consisted of a cylindrical shell made up of the stainless steel, and the spiral wound membranes were installed in the shell. A cylindrical feed tank of 30 L capacity was used for storing the water required for the experimentation. The flow rates of the permeate and the concentrate streams were indicated by the rotameters while the pressures were shown by the mounted pressure gauges. A variable frequency drive controlled the speed of the motor. This helped to vary the flow rates and the pressures.

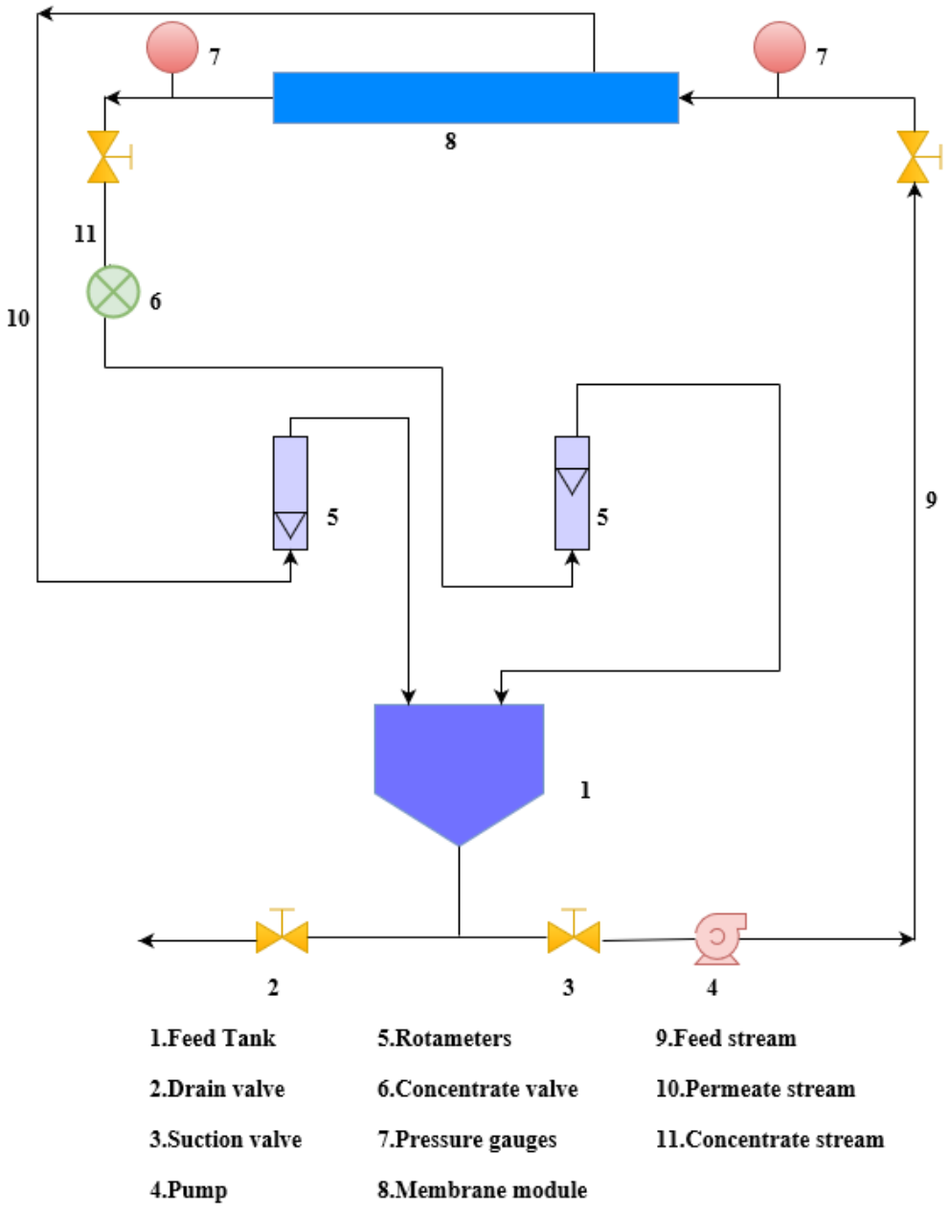

Fig. 2. The schematic diagram of perma® plant.

3.3. Experimental procedure

The wastewater samples of 20–100 mg/L of Mn(II) were prepared by dissolving the required amount of manganese sulfate. Before performing the actual experiments to remove manganese, the HPA-400 membrane was exposed to the deionized (DI) water for 20 min at the transmembrane pressure of 12 bar for stabilization purpose. It helped to avoid the probable membrane compaction throughout the experimentation. The experiments were conducted in a batch circulation mode. The permeate and the concentrate samples were collected at the end of every 15 min. Both streams of the permeate and the concentrate were back circulated to the feed tank to maintain a constant feed concentration. After each set of the experiments, the setup was washed with the deionized water for 20 min. This helped the system to remain clean. After every set of the experiment, the pure water permeability (PWP) was measured to confirm that the original membrane PWP was preserved. The experiments were performed at the various feed concentrations (20–100 mg/L), the transmembrane pressures (5–9 bar), and the feed flow rates (0.713–1.050 L/min). For every reading, the corresponding observed salt rejection (R_o) and the permeate volume flux (J_v) were measured. The separation performance of the membrane was calculated as:

$$\%R_o = \left[1 - \left(\frac{C_p}{C_f}\right)\right] \times 100 \tag{19}$$

where C_p is the metal ion concentration in the permeate stream and C_f is its concentration in the feed. To prevent the biological fouling, the membrane was washed with 1% sodium meta-bisulphite at the end of the experimental runs.

3.4. Analyses

The manganese ion concentrations were measured by an atomic absorption spectrophotometer (Model: AA-201, Chemito, India) using the standard procedures. A calibration curve between the absorbance and the sample concentrations was prepared. In order to prepare the calibration curve, standard manganese metal solution (1000 mg/L) was used as a stock solution. From the stock solution, 5 dilute solutions according to the given range of an atomic absorption spectrophotometer for the manganese metal detection were prepared. The concentrations of these solutions were 1–5 mg/L. The absorbance of these solutions was measured at 279.5 nm wavelength as the most sensitive wavelength for the manganese metal and then plotted against the concentrations of the solutions. During the experiments, samples of the permeate and the concentrate solutions were collected at every 15min time interval for the analysis.

3.5. Design of experiments

The most important stage in the design of experiments lies in the selection of control factors. Taguchi creates a standard orthogonal array (OA) to accommodate this requirement [37]. Application of OA reduces the number of experiments required to determine the influence of various operating parameters over the process output [38]. The Taguchi technique provides much reduced variance for the experiments with an optimum set of process control parameters. Thus,it offers a simple and systematic approach to optimize design for performance, quality and cost [39–42].

In this research work,the Taguchi parameter design methodology was used. According to this design, an orthogonal array, L_9 (three factors and three levels) of nine trials was employed. The three factors were the feed concentration (A), the transmembrane pressure (B), and the feed flow rate (C) with levels as 1,2, and 3. The factors and their levels are given in Table 2. For the analysis of the results and to develop a statistical model, MINITAB® 18 software was used.

4. Results and discussion

4.1.The water permeability of membrane

The pure water permeability coefficient (L_p) characterizes the water flow across the membrane. Before conducting the metal rejection experiments, the permeability of the membrane to the deionized water was calculated at 25°C. The pure water permeability coefficient of the membrane was obtained as a slope of the plot of the pure water flux against the transmembrane pressure. From Fig. 3, the L_p value was found to be 8.32 L/h·m^2 bar. This is in the range of the values for the NF membranes [27,43].

Table 2
Factors and levels for Taguchi design of experiment

Factors	Levels		
	1	2	3
(A) Feed concentration (mg/L)	20	60	100
(B) Transmembrane pressure (bar)	5	7	9
(C) Feed flow rate (LPM)	0.713	0.927	1.050

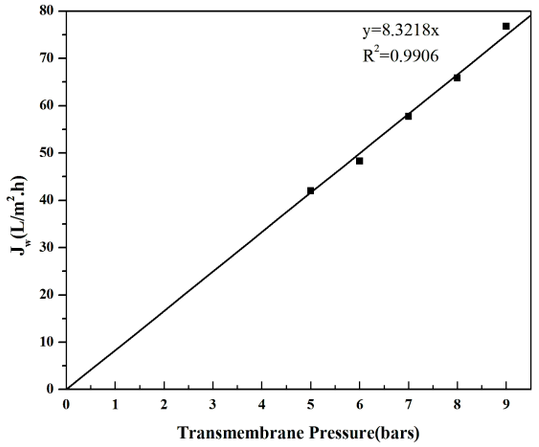

Fig. 3. Pure water flux as a function of transmembrane pressure at T = 25°C.

4.2. Effect of transmembrane pressure

It was observed from Fig. 4 that with the increase in transmembrane pressure, the permeate flux increased. In Fig. 5, the relation between the permeate flux and the metal rejection at the various feed concentrations (20–100 mg/L) and the transmembrane pressures (5–9 bar) is shown. Each data series of the feed concentration indicates the increasing permeate flux with the increasing transmembrane pressure. It can be seen from Fig. 5 that with the increase in the permeate flux, the rejection of metal increased slightly for the increasing feed concentrations. It was also observed that the rejection increased with the increase in the transmembrane pressures from 5 to 9 bar (Fig. 5). It is related to the 'dilution effect' that is as the transmembrane pressure increases, the convective transport of the water becomes predominant over the diffusive transport of the solute. This phenomenon results in a lower solute concentration in the permeate and thus, the rejection of manganese increases with the transmembrane pressures. Furthermore, it was seen from Fig. 4 that the permeate flux was not increasing linearly with the transmembrane pressures for the given feed concentrations. This may be due to the concentration polarization at a minor level.

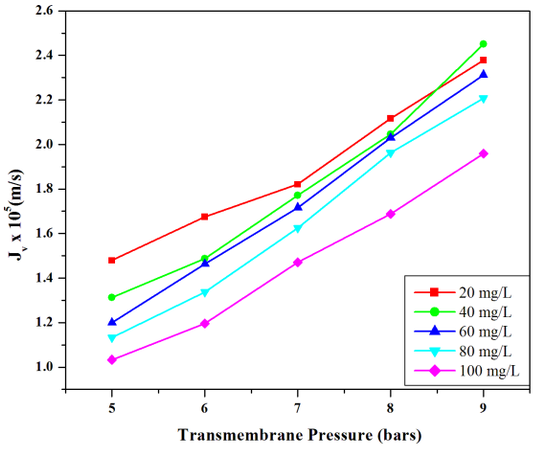

Fig. 4. Permeate flux at various transmembrane pressures for different feed concentrations.

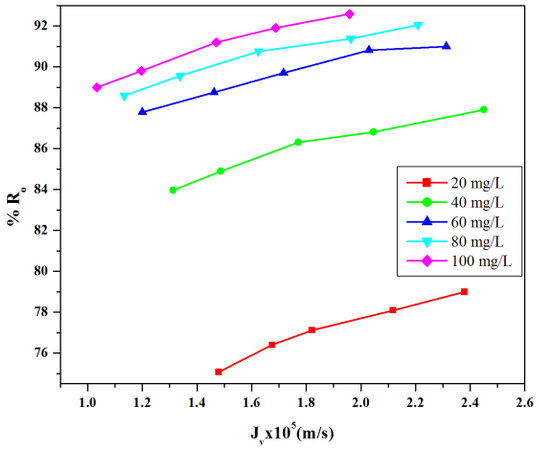

Fig. 5. Relation between rejection and permeate flux at various feed concentrations.

4.3. Effect of initial concentration

Fig. 4 explains the effect of the metal concentration (20–100 mg/L) on the permeate flux of the membrane. This figure indicated that the permeate flux declined with the increasing feed concentration for all the transmembrane pressures during the experiment. This can be explained as with the increase in the feed concentration, the concentration difference across the membrane increases, which results in an increase in the osmotic pressure. The increased osmotic pressure causes a drop in the permeate flow. Also,the adsorption or the deposition of the solute on the membrane surface may affect the effective membrane pore size. Thus, the lowest flux obtained at the transmembrane pressure of 5 bar and the feed concentration of 100 mg/L was 1.033×10^{-5} m/s.

Fig. 5 depicts that the initial feed concentration of manganese influenced the rejection. As the feed concentration increased, the rejection of manganese increased. It was found that the solute concentration at the membrane surface was increased with the increase in the feed concentration. The resulting concentrated layer at the membrane surface exerted the additional resistance to the solute transport and consequently the rejection increased with the increasing feed concentration.

Fig. 6 presents the manganese concentration in the permeate during the experiment at the various feed concentrations and the transmembrane pressures. The lowest permeate concentration was 4.2 mg/L at the transmembrane pressure of 9 bar and the feed concentration of 20 mg/L. It indicates the required purity of the permeate stream up to which the wastewater of various concentrations can be concentrated.

4.4. Effect of feed flow rate

Fig. 7 shows the rejection of manganese at the various feed flow rates. The increase in the metal rejection with

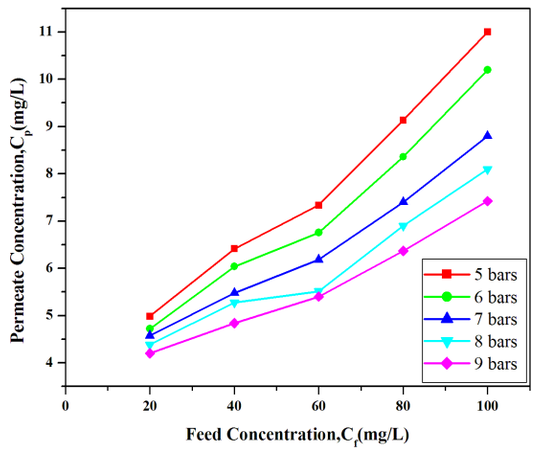

Fig. 6. Permeate concentration vs feed concentration.

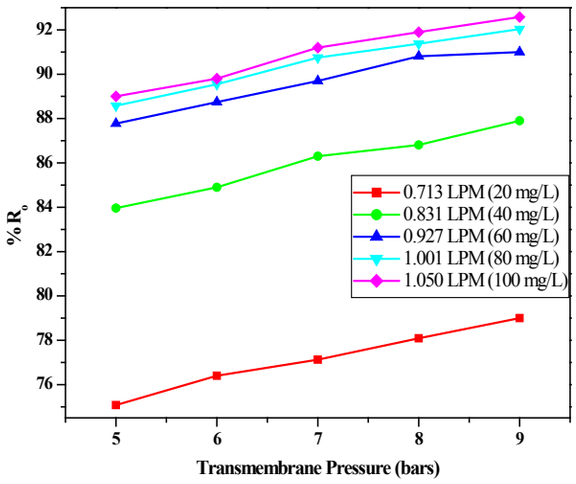

Fig. 7. Effect of feed flowrate on rejection at various concentrations.

an increase in the feed flow rates is due to the increase in the mass transfer coefficients. This increase in mass transfer coefficients may be due to the increase in the Reynolds number.

4.5. Statistical analysis

Table 3 shows the L_9 orthogonal array where factors A, B, C are arranged in column 1, 2, and 3, respectively. Each row of the orthogonal array represents a run with a specific set of factor levels in the experiments to be conducted. Based on the data obtained from the experiments, the statistical analysis of variance (ANOVA) was performed to determine the significant effect of each operating factor on the response variable. The analysis was conducted at 95% confidence level (level of significance, $\alpha = 0.05$). The obtained ANOVA results are summarized in Table 4. The variable having the higher F-value and the smaller P-value than the other variables is more significant variable. The P-value should be less than the selected confidence level (0.05) to become a significant factor. It can be seen from Table 4 that the feed concentration provided the most significant effect on the metal rejection, followed by the transmembrane pressure and the feed flow rate having P-value 0.00001, 0.00048, and 0.02081, respectively.

Taguchi method emphasizes on the study of the response variation using the signal-to-noise (S/N) ratio, resulting in the minimization of the response variation due to uncontrollable parameter. The metal rejection was considered as the response variable with the concept of "the larger-the-better". Based on the analysis of the S/N ratio, the optimal performance for the metal rejection was found at 100 mg/L feed concentration (level 3), 9 bar transmembrane pressure (level 3), and 1.050 LPM feed flow rate (level 3) (Table 5). Fig. 8 shows the main effect plot of S/N ratios.

Furthermore, a regression model was developed for predicting the metal rejection as a function of the feed concentration (A), the transmembrane pressure (B), and the feed flow rate (C) as follows:

Table 3
Taguchi L_9 orthogonal array

Run	Factors levels			Rejection (%)
	A	B	C	
1	1	1	1	75.07
2	1	2	2	77.74
3	1	3	3	80.00
4	2	1	2	87.77
5	2	2	3	90.50
6	2	3	1	90.62
7	3	1	3	89.00
8	3	2	1	90.00
9	3	3	2	91.54

$$\%\ \text{Rejection} = 58.06 + 0.5876 \times A + 0.86 \times B + 3.576 \times C - 0.003587 \times A^2 \quad (20)$$

The model F-value of 495.83 and the corresponding value of prop > F (0.00001) suggested that the model was significant. The statistical model of metal rejection (Table 4) was in good agreement with the experimental data as the value of regression coefficient (R^2), 99.80%, was close to 1. Predicted R^2 of 99.09%was in reasonable agreement with the adjusted R^2 of 99.60%. The ranking of the significant factors was A > A^2 > B > C. The membrane rejection ability was contributed by the first-order effect of the feed concentration (A), the transmembrane pressure (B), the feed flow rate (C), and the quadratic effect of the feed concentration (A^2). The model showed a standard error (S) of 0.4035. S is the measure of deviation of observed rejection (% R) from the regression line. It is supposed that the lower the S value, the better the generated model. In this study, a confirmatory experiment was conducted by applying the optimal levels of the process parameters and the metal rejection was found as 92.58%.

A plot of the normal% probability vs. residual is shown in Fig. 9 for the metal rejection. The normal probability plot of the residuals is an important diagnostic tool in the residual analysis. It is used to check the normal distribution of errors and their independence from each other. It was observed from the figure that most of the residuals were close to the diagonal line suggesting no noticeable sign of non-normality of the experimental results. A plot of standardized residual vs. fitted value (Fig. 10) showed an equal scatter around the x-axis. It indicates the absence of any recognized pattern. From the figure, it is proved that the model proposed by the analysis is adequate. The predicted values of the response variable vs. actual values are shown in Fig. 11. The goodness-of-fit of the model was checked through the correlation coefficient (R^2). The figure demonstrated that the empirical model was reliable to predict the membrane performance in terms of metal rejection.

4.6. Theoretical modeling

4.6.1. Determination of transport parameters

There are limitations to the CFSD model as it is used for the homogeneous and nonporous membrane surface

Table 4
Analysis of variance for responses

Source	d_f	Adj SS	Adj MS	F-Value	P-Value
Regression	4	323.038	80.759	495.83	0.00001
(A) Feed concentration (mg/L)	1	118.383	118.383	726.83	0.00001
(B)Transmembrane pressure(bar)	1	17.750	17.750	108.98	0.00048
(C)Feed flow rate (LPM)	1	2.232	2.232	13.70	0.02081
(A^2) [Feed concentration (mg/L)]^2	1	65.872	65.872	404.43	0.00004
Error	4	0.652	0.163		
Total	8	323.689			

d_f= Degrees of Freedom; SS = Sum of Squares; MS = Mean Square error; F = F-value; P = P-value; Note: The p-values less than 0.05 are significant.

Table 5
S/N ratio values for response variable

Level	Feed concentration (mg/L)	Transmembrane pressure (bar)	Feed flow rate (LPM)
1	37.80	38.46	38.58
2	39.05	38.68	38.64
3	39.10	38.81	38.73
Delta	1.31	0.36	0.15
Rank	1	2	3

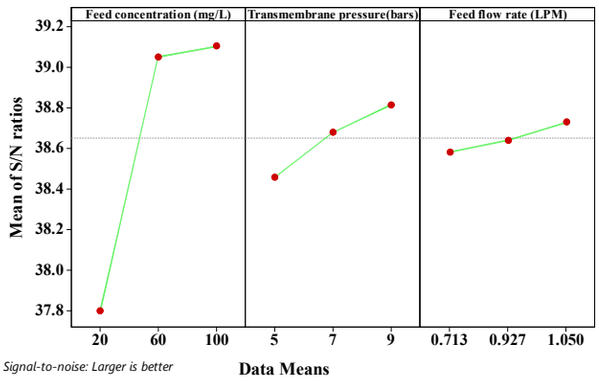

Fig. 8. Main effects plot for S/N ratio.

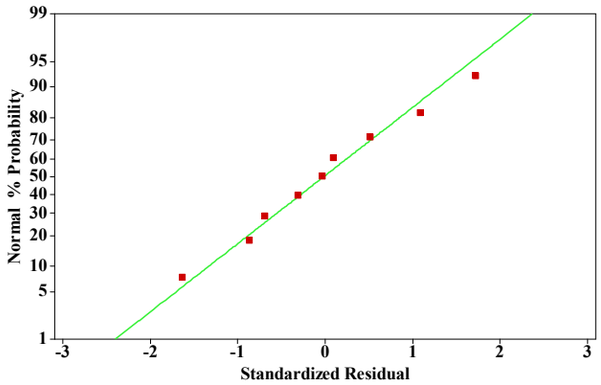

Fig. 9. Normal probability plot.

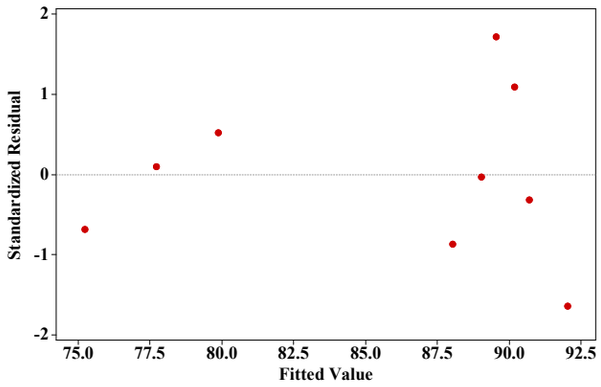

Fig. 10. Residual vs fits plot.

layer. Also, it is applicable when the separation is close to 1.0. Moreover, this model assumes each species must first dissolve into the membrane before diffusing through and all the transport occurs by the diffusion only [44]. However, this is not true for nanofiltration. Hence, the CFSK model was used for the further calculations. For the estimation of the parameters of the Eq. (16), the experimental data of R_o and J_v obtained at the various transmembrane pressures,but a constant feed concentration and a constant feed flow rate were applied. The regression was done using a nonlinear curve fitting technique. The MATLAB® (R2014a, The MathWorks Inc.,USA) function *lsqcurvefit* was used to obtain the model parameters. The parameters estimated from Eq. (16) were used to calculate the rejection coefficient of manganese from the model. This calculated rejection and the experimental rejection were compared as shown in Fig. 12. It can be observed from Fig. 12 that the model predictions for the rejection were in good agreement with the experimental results. The membrane transport parameters estimated from Eq. (16) are given in Table 6.

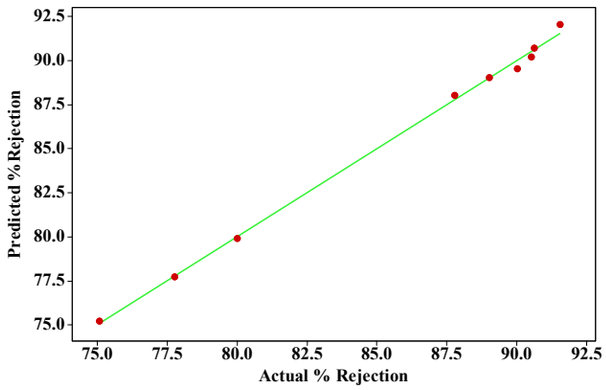

Fig. 11. Plot of predicted vs actual metal rejection.

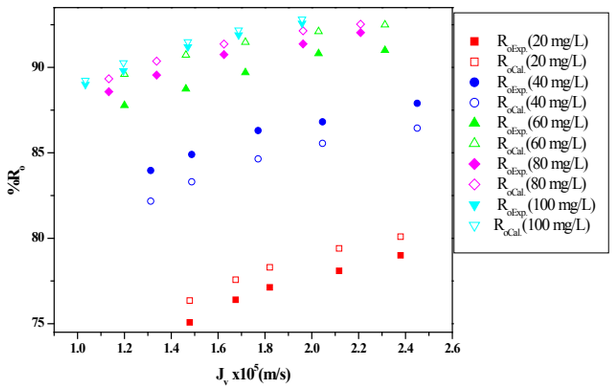

Fig. 12. Comparison between $Ro_{exp.}$ and $Ro_{cal.}$ as a function of Permeate volume flux for combined–film theory-Spiegler-Kedem model.

Table 6
Parameter estimated using non-linear regression method for CFSK model for manganese ions

Set no.	Feed conc. (mg/L)	CFSK model[a]		
		σ	$P_M \times 10^6$ (m/s)	$k \times 10^5$ (m/s)
1	20	0.9964	3.0	3.6
2	40	0.9922	2.0	4.1
3	60	0.9906	1.0	4.5
4	80	0.9900	1.0	4.8
5	100	0.9978	1.0	5.0

[a]CFSK is combined–film theory-Spiegler-Kedem model

4.6.2. Development of Sherwood correlation

The mass transfer coefficient, k is mainly a function of the feed flow velocity, the module shape and dimensions, and the solute system [44]. Most of the mass transfer models used to describe the membrane processes apply the Sherwood correlation. The Sherwood correlation for a fully developed turbulent flow is [45].

Table 7
Comparison of experimental and calculated k values

Set no.	$k_{exp.} \times 10^5$ (m/s)	$k_{cal} \times 10^5$ (m/s)	% error in k
1	3.60	3.59	0.0875
2	4.10	4.09	0.0555
3	4.50	4.49	0.1136
4	4.80	4.79	0.0260
5	5.00	4.99	0.1202

$$Sh = \frac{k.d_h}{D} = a.\mathrm{Re}^b.Sc^c = a.\left(\frac{u.d_h}{\nu}\right)^b.\left(\frac{\nu}{D}\right)^c \quad (21)$$

Also, for a fully developed laminar flow, the equation is [46].

$$Sh = \frac{k.d_h}{D} = a.\mathrm{Re}^b.Sc^c.\left(\frac{d_h}{L}\right)^d = a.\left(\frac{u.d_h}{\nu}\right)^b.\left(\frac{\nu}{D}\right)^c.\left(\frac{d_h}{L}\right)^d \quad (22)$$

where Sh is the Sherwood number, Re is the Reynolds number, Sc is the Schmidt number. Also, u is the cross-flow velocity (m/s), ν is the kinematic viscosity (m^2/s), D is the diffusion coefficient of solute (m^2/s), L is the channel length (m) and d_h is the hydraulic diameter (m). The unknown parameters a, b, c, and d are to be calculated after experimental runs only [47,48].

For the spacer filled spiral wound RO membrane channel, Schock and Miquel developed the Sherwood correlation as [49]:

$$Sh = \frac{k.d_h}{D} = 0.065.\mathrm{Re}^{0.875}.Sc^{0.25} \quad (23)$$

As the flow was laminar, the Sherwood correlation for the spiral wound membrane module under the studies was obtained as:

$$Sh = \frac{k.d_h}{D} = 0.663.\mathrm{Re}^{0.849}.Sc^{0.418}.\left(\frac{d_h}{L}\right)^{0.288} \quad (24)$$

This was done by the nonlinear fitting of Eq. (22) with the MATLAB function *nlinfit*. The k values estimated from the CFSK model, Eq. (16) and the Sherwood correlation, Eq. (24) are compared in Table 7 and they are in good agreement.

4.6.3.Calculation of enrichment factors and concentration polarization modulus

Concentration polarization is a natural consequence of the selectivity of a membrane and is one of the significant control factors influencing the system design. The enrichment factor, E is dependent on the feed concentration. On the other hand, when the boundary layer is not present, the enrichment factor E_o is dependent on the surface concentration of the membrane. The enrichment factors (E_o and E) along with the concentration polarization modulus (C_{A2}/C_{A1}) for the HPA-400 membrane are given in Table 8 (at transmembrane pressure 5 bar). It can

Table 8
Representative values of the enrichment factors (E_o and E), and concentration polarization modulus (C_{A2}/C_{A1}) for HPA-400 NF membrane at various concentrations (TMP 5 bar)

Set no.	Feed concentration (mg/L)	Enrichment factors		Concentration polarization modulus (C_{A2}/C_{A1})	Peclet number (J_v/k)
		E_o	E		
1	20	0.1804	0.2492	1.3814	0.4108
2	40	0.1217	0.1603	1.3167	0.3201
3	60	0.0964	0.1222	1.2682	0.2666
4	80	0.0924	0.1142	1.2359	0.2361
5	100	0.0913	0.1100	1.2043	0.2066

be observed from Table 8 that the membrane surface concentration of the solute was 1.2–1.3 times higher than in the feed solution.

The equilibrium between the convective transport and the diffusive transport in the boundary layer is described by the term (J_v/k). This dimensionless number signifies the ratio of the convective transport, J_v and the diffusive transport, k. It is normally defined as the Peclet number [35]. The Peclet numbers for the HPA-400 membrane at the various feed concentrations and at the transmembrane pressure of 5 bar are also shown in Table 8. At higher values of the Peclet numbers ($J_v>>k$), the convective flux becomes predominant over the diffusive flux in the boundary layer showing a large value of the concentration polarization modulus. At smaller values of the Peclet numbers ($J_v<<k$),convective flux is well controlled by the diffusive flux in the boundary layer. In this situation, the concentration polarization modulus turns near to unity [35]. It can be observed from Table 8 that at the transmembrane pressure of 5 bar, the value of the Peclet number is between 0.20 and 0.41. It has the maximum value between 0.39 and 0.66 at the transmembrane pressure of 9 bar(data not given in Table 8). This shows that the concentration polarization increases with the transmembrane pressure.

5. Conclusions

The present study validates that NF is an effective membrane separation technique to remove manganese from the synthetic wastewater. The pure water permeability coefficient of the membrane was found to be 8.32 L/h·m² bar. Initially the operating parameters, such as, the initial feed concentration, the transmembrane pressure, and the feed flow rate were considered to estimate the role in the metal rejection and the permeation flux. As the transmembrane pressure increased, the permeate flux and the metal rejection increased. Also, it was observed that with the increase in initial feed concentration, the permeate flux slightly decreased and the metal rejection increased. In addition, with the increase in the feed flow rate, manganese rejection increased. In order to find the significant operating parameters, Taguchi method was used. The analyses of the results in terms of S/N ratio, and ANOVA showed that the feed concentration was the most influencing operating parameter, followed by the transmembrane pressure and the feed flow rate. The maximum rejection of the metal was found to be 92.58% at the optimum level (initial feed concentration of 100 mg/L, the transmembrane pressure of 9 bar, and the feed flow rate of 1.050 LPM) of the three factors. As well, a statistical model was developed and it showed good validity with the experimental data (error less than 0.54%). Furthermore, a theoretical modeling study was performed using the combined–film theory-Spiegler-Kedem model (CFSK) as the membrane transport model. The model predicted well the experimental data with the error less than ± 2.5%.The Sherwood correlation was also developed for the spiral wound membrane module under the studies. The k values estimated from the CFSK model and from the Sherwood correlation were compared and they were in good agreement with the error less than ±1%. The enrichment factors, the concentration polarization modulus, and the Peclet numbers have been discussed and calculated for the membrane under study.

Acknowledgements

The corresponding author acknowledges AICTE, New Delhi, India to provide the financial support for the research equipment and chemicals under research proposal scheme (File No. 8023/BOR/RID/RPS-8/2009-10).

Nomenclature

a	—	Constant in Eq. (20)
A	—	Permeability parameter in Eq. (6) (mol/cm² bar)
b	—	Constant in Eq. (20)
c	—	Constant in Eq. (20)
C_{Ai}	—	Concentration of $\underline{A}$ at any location i (mg/L)
C_p	—	Permeate concentration (mg/L)
C_f	—	Feed concentration (mg/L)
d	—	Constant in Eq. (21)
d_h	—	Hydraulic diameter (m)
D	—	Diffusivity (m²/s)
$(D_{AM}K/\delta)$	—	Solute transport parameter (m/s)
D_{AB}	—	Diffusivity of solute A in solvent B (m²/s)
D_{AM}	—	Diffusivity of solute A in membrane (m²/s)
E	—	Enrichment factor defined as C_{A3}/C_{A1}
E_o	—	Enrichment factor in the absence of boundary layer defined as C_{A3}/C_{A2}
F	—	Factor in Eq. (13)
Jv	—	Permeate volume flux (m/s)
J_w	—	Pure water flux (L/m²h)

k — Mass transfer coefficient (m/s)
K — Solute partition coefficient
l — Thickness of the concentration boundary layer (m)
L — Channel length (m)
L_p — Pure water permeability coefficient (L/h·m^2 bar)
Δp — Pressure difference across the membrane (bar)
P_M — Overall permeability coefficient (m/s)
Q — Feed flow rate (L/min)
R — True rejection
Re — Reynolds number
Ro — Observed solute rejection
Sc — Schmidt number
Sh — Sherwood number
TMP — Transmembrane pressure (bar)
u — Cross-flow velocity (m/s)
v — Kinematic viscosity (m^2/s)

Greek letters

δ — Effective thickness of a membrane (m)
$\Delta\pi$ — Osmotic pressure difference across the membrane (bar)
σ — Reflection coefficient

Subscripts

A — Solute
B — Solvent
M — Membrane
1 — Feed Solution
2 — Boundary layer solution
3 — Permeate solution

Conflict of interest

No conflict of interest

References

[1] F. Fu, Qi Wang, Removal of heavy metal ions from wastewaters: A review, J. Environ. Manage., 92 (2011) 407–418.
[2] P. Patnaik, Handbook of inorganic chemicals, McGraw-Hill, New York, 2002.
[3] H. Xuwen, Y. Huimin, H. Yong, Treatment of mine water high in Fe and Mn by modified manganese sand, Min. Sci. Tech., 20 (2010) 0571–0575.
[4] C.L. Beh, T.G. Chuah, M.N. Nourouzi, T.S.Y. Choong, Removal of heavy metals from steel making wastewater by using electric arc furnace slag, E-J. Chem., 9(4) (2012) 2557–2564.
[5] World Health Organization (2011), Manganese in Drinking-water, Background Document for Development of WHO Guidelines for drinking water quality, WHO, Geneva, Switzerland.
[6] USEPA, "Drinking Water Health Advisory for Manganese", U.S. Environmental Protection Agency, Office of Water, Washington, DC EPA-822-R-04-003, 2004.
[7] D. Allen, K. Pelude, Dissolved Manganese in Drinking Water on the Gulf Islands: Occurrence and Toxicity, Burnaby, Department of Earth Sciences, Simon Fraser University, B.C. V5A 1S6, 2001.
[8] P. Brandhuber, S. Craig, M. Friedman, A. Hill, S. Booth, A. Hanson, (2015) Legacy of Manganese Accumulation in Water Systems, Water Research Foundation, Report #4314, Denver, CO.
[9] D.S. Patil, S.M. Chavan, J.U. Kennedy, A review of technologies for manganese removal from wastewaters, J. Environ. Chem. Engg., 4 (2016) 468–487.
[10] R.A. Duarte, A.C. Ladeira,Study of manganese removal from mining effluent, mine water-managing the challenges (IMWA 2011, Aachen, Germany) (2011) 297–300.
[11] R.J. Lovett, Removal of manganese from acid mine drainage, J. Environ. Quality, 26(4) (1997) 1017–1024.
[12] A.O. Aguiar, R.A. Duarte, A.C.Q. Ladeira, The application of MnO_2 in the removal of manganese from acid mine water, Water Air Soil Pollut., 224 (2013) 1690. DOI: 10.1007/s11270-013-1690-2.
[13] A.M. Silva, F.L.S. Cruz, R.M.F. Lima, M.C. Teixeira, V.A. Leão, Manganese and limestone interactions during mine water treatment, J. Hazard. Mater., 181 (2010) 514–520.
[14] D. Ellis, C. Bouchard, G. Lantagne, Removal of iron and manganese from groundwater by oxidation and microfiltration, Desalination, 130 (2000) 255–264.
[15] Z. Teng, J.Y. Huang, K. Fujita, S. Takizawa, Manganese removal by hollow fiber micro-filter. Membrane separation for drinking water, Desalination, 139 (2001) 411–418.
[16] D. Mourato, C. Smith, Proc., 6th Workshop on Drinking Water, AQTE, Montreal, 1994, pp. 705–716.
[17] P. Côté, D. Mourato, C. Güngerich, J. Russell, E. Houghton, Immersed membrane filtration for the production of drinking water: case studies, ISWA Conference, Membranes in Drinking and Industrial Water Production, Amsterdam, 1998.
[18] I.A. Katsoyiannis, A.I. Zouboulis, Biological treatment of Mn(II) and Fe(II) containing groundwater: kinetic considerations and product characterization, Water Res., 38 (2004) 1922–1932.
[19] S.M. Bamforth, D.A.C. Manning, I. Singleton, P.L. Younger, K.L. Johnson, Manganese removal from mine waters—investigating the occurrence and importance of manganese carbonates, Appl. Geochem., 21(8) (2006) 1274–1287.
[20] M. Bodzek, K. Konieczny, A. Kwiecińska, Application of membrane processes in drinking water treatment–state of art, Desal. Water Treat., 35 (2011) 164–184.
[21] H.A. Qdaisa, H. Moussa, Removal of heavy metals from wastewater by membrane processes: a comparative study, Desalination, 164 (2004) 105–110.
[22] N. Hilal, H. A1-Zoubi, N.A. Darwish, A.W. Mohammad, M. Abu Arabi, A comprehensive review of nanofiltration membranes: Treatment, pretreatment, modeling, and atomic force microscopy, Desalination, 170 (2004) 281–308.
[23] Ministry of Environment & Forests, Global good practices in industrial wastewater treatment and disposal/reuse, with special reference to common effluent treatment plants, Central Pollution Control Board, Govt. of India, 2015. www.cpcb.nic.in/Report_CETP_GGP.pdf.
[24] S. Chaturvedi, P.N. Dave, Removal of iron for safe drinking water, Desalination, 303 (2012) 1–11.
[25] R.S. Harisha, K.M. Hosamani, R.S. Keri, S.K. Nataraj, T.M. Aminabhavi, Arsenic removal from drinking water using thin film composite nanofiltration membrane, Desalination, 252 (2010) 75–80.
[26] Y. Ku, Shi-Wei Chen, Wen-Yu Wang, Effect of solution composition on the removal of copper ions by nanofiltration, Sep. Purif. Technol., 43 (2005) 135–142.
[27] G.T. Ballet, L. Gzara, A. Hafiane, M. Dhahbi, Transport coefficients and cadmium salt rejection in nanofiltration membrane, Desalination, 167 (2004) 369–376.
[28] M. Taleb-Ahmed, S. Taha, R. Maachi, G. Dorange, The influence of physico-chemistry on the retention of chromium ions during nanofiltration, Desalination, 145 (2002) 103–108.
[29] N.B. Frare`s, S. Taha, G. Dorange, Influence of the operating conditions on the elimination of zinc ions by nanofiltration, Desalination, 185 (2005) 245–253.
[30] C.V. Gherasim, P. Mikulášek, Influence of operating variables on the removal of heavy metal ions from aqueous solutions by nanofiltration, Desalination, 343 (2014) 67–74.

[31] Z.V.P. Murthy, S.K. Gupta, Estimation of mass transfer coefficient using a combined nonlinear membrane transport and film theory model, Desalination, 109 (1997) 39–49.
[32] U. Merten, Transport properties of osmotic membranes, in: U. Merten (Ed.), Desalination by Reverse Osmosis, MIT Press, Cambridge, MA, 1966, pp. 15–24.
[33] W. Pusch, Determination of transport parameters of synthetic membranes by hyperfiltration experiments. Part I. Derivation of transport relationship from linear relations of thermodynamics of irreversible processes, Ber. Bunsen. Phys. Chem., 81 (1977) 269–276.
[34] O. Kedem, K. Spiegler, Thermodynamics of hyperfiltration (reverse osmosis): criteria for efficient membranes, Desalination, 1 (1966) 311–326.
[35] R.W. Baker, Membrane Technology, and Applications, 2nded., John Wiley & Sons Inc., NJ, USA, 2004.
[36] M. Mulder, Basic Principles of Membrane Technology, 2nded., Kluwer Academic Publishers, Dordrecht, 1996.
[37] S.S. Madaeni, S. Koocheki, Application of Taguchi method in the optimization of wastewater treatment using spiral-wound reverse osmosis element, Chem. Eng. J., 119 (2006) 37–44.
[38] D. Allende, D. Pando, M. Matos, C.E. Carleos, C. Pazos, J.M. Benito, Optimization of a membrane hybrid process for oil-in-water emulsions treatment using Taguchi experimental design, Desal. Water Treat., 57(11) (2016) 4832–4841.
[39] G. Taguchi, in: Introduction to Quality Engineering, Asian Productivity Organization, Tokyo, 1990.
[40] P.G. Ross, in: Taguchi Techniques for Quality Engineering, 2nd ed., McGraw-Hill, New York, 1996.
[41] S.H. Park, Robust design and Analysis for Quality Engineering, Chapman & Hall, London, 1996.
[42] M.S. Phadke, Quality Engineering Using Robust Design, Prentice-Hall, USA, 1989.
[43] Z.V.P. Murthy, A. Choudhary, Separation of cerium from feed solution by nanofiltration, Desalination, 279 (2011) 428–432.
[44] J.M. Dickson, H. Mehdizadeh, Overview of reverse osmosis for chemical engineers part 1: Fundamentals of membrane mass transfer, J. Eng. Islam. Repub. Iran, 1 (1988) 163–179.
[45] V. Gekas, B. Hallström, Mass transfer in the membrane concentration polarization layer under turbulent crossflow: I. Critical literature review and adaptation of existing Sherwood correlations to membrane operations, J. Membr. Sci., 30(2) (1987) 153–170.
[46] R.B. Bird, W.E. Stewart, E.N. Lightfoot, Transport Phenomena, first ed., John Wiley & Sons, Inc., New York, 1960.
[47] T.Y. Qiu, P.A. Davies, Concentration polarization model of spiral-wound membrane modules with application to batch mode RO desalination of brackish water, Desalination, 368 (2015) 36–47.
[48] B. Shi, P. Marchetti, D. Peshev, S. Zhang, A.G. Livingston, Performance of spiral-wound membrane modules in organic solvent nanofiltration–Fluid dynamics and mass transfer characteristics, J. Membr. Sci., 494 (2015) 8–24.
[49] G. Schock, A. Miquel, Mass-transfer and pressure loss in spiral wound modules, Desalination, 64 (1987) 339–352.